1   **Biomass Burning Aerosol as a Modulator of Droplet Number in the Southeast**

2   **Atlantic Region**

4   Mary Kacarab[1], K. Lee Thornhill[2], Amie Dobracki[3], Steven G. Howell[3], Joseph R.

5   O'Brien[4], Steffen Freitag[3], Michael R. Poellot[4], Robert Wood[5], Paquita Zuidema[6], Jens

6   Redemann[7], and Athanasios Nenes[1,8,9]

8   [1]School of Earth & Atmospheric Sciences, Georgia Institute of Technology, Atlanta, GA,

9   30332, USA

10   [2]NASA Langley Research Center, Hampton, VA, 23666, USA

11   [3]Department of Oceanography, University of Hawaii, Honolulu, HI, 96822, USA

12   [4]Atmospheric Sciences Department, University of North Dakota, Grand Forks, ND,

13   58202, USA

14   [5]Atmospheric Sciences, University of Washington, Seattle, WA, 98195, USA

15   [6]Department of Atmospheric Sciences, Rosenstiel School of Marine and Atmospheric

16   Science, University of Miami, Miami, FL, 33149, USA

17   [7]School of Meteorology, University of Oklahoma, Norman, OK, 73072, USA

18   [8]Institue for Chemical Engineering Sciences, Foundation for Research and Technology

19   Hellas, Patras, GR-26504, Greece

20   [9]Laboratory of Atmospheric Processes and their Impacts, School of Architecture, Civil

21   and Environmental Engineering, Ecole Polytechnique Federale de Lausanne, Lausanne,

22   CH-1015, Switzerland

24   Corresponding Author: Athanasios Nenes (athanasios.nenes@epfl.ch)

27   **Abstract**

28   The southeastern Atlantic (SEA) and its associated cloud deck, off the west coast of

29   central Africa, is an area where aerosol-cloud interactions can have a strong radiative

30   impact. Seasonally, extensive biomass burning (BB) aerosol plumes from southern Africa

31   reach this area. The NASA ObseRvations of Aerosols above Clouds and their

32   intEractionS (ORACLES) study focused on quantitatively understanding these

33   interactions and their importance. Here we present measurements of cloud condensation

34   nuclei (CCN) concentration, aerosol size distribution, and characteristic vertical updraft

35   velocity ($w*$) in and around the marine boundary layer (MBL) collected by the NASA P-

36   3B aircraft during the August 2017 ORACLES deployment. BB aerosol levels vary

37   considerably but systematically with time; high aerosol concentrations were observed in

38   the MBL (800-1000 cm^{-3}) early on, decreasing mid-campaign to concentrations between

39   500-800 cm^{-3}. By late August and early September, relatively clean MBL conditions were

40   sampled (<500 cm^{-3}). These data then drive a state-of-the-art droplet formation

41   parameterization, from which the predicted cloud droplet number and its sensitivity to

42   aerosol and dynamical parameters are derived. Droplet closure was achieved to within

43   20%. Droplet formation sensitivity to aerosol concentration, $w*$, and the hygroscopicity

44   parameter, κ, vary and contribute to the total droplet response in the MBL clouds. When

45   aerosol concentrations exceed ~900 cm^{-3} and maximum supersaturation approaches

46   0.1%, droplet formation in the MBL enters a "velocity-limited" droplet activation regime,

47   where cloud droplet number responds weakly to CCN concentration increases. Below

48   ~500 cm^{-3}, in a "clean" MBL, droplet formation is much more sensitive to changes in

49   aerosol concentration than to changes in vertical updraft. In the "competitive" regime,

50   where the MBL has "intermediate" pollution (500-800 cm^{-3}), droplet formation becomes

51   much more sensitive to hygroscopicity (κ) variations than for clean and polluted

52   conditions. Higher concentrations increase the sensitivity to vertical velocity by more

53   than ten-fold. We also find that characteristic vertical velocity plays a very important role

54   in driving droplet formation in a more polluted MBL regime, in which even a small shift

55   in $w*$ may make a significant difference in droplet concentrations. Identifying regimes

56   where droplet number variability is primarily driven by updraft velocity and not aerosol

57   concentration is key for interpreting aerosol indirect effects, especially with remote

58   sensing. Droplet number responds proportionally to changes in characteristic velocity,

59   offering the possibility of remote sensing of w^* under velocity-limited conditions.

60

1.   Introduction

Aerosol particles affect the planetary radiative balance by directly absorbing and scattering radiation. They also provide the nuclei upon which cloud droplets and ice crystals form; variations thereof can profoundly impact cloud formation, precipitation, and the hydrological cycle (Boucher et al., 2013; Myhre et al., 2013). These aerosol impacts are thought to be important but uncertain modulators of regional and global scale climate. The interactions of aerosols with clouds are especially uncertain, and affect estimates of equilibrium climate sensitivity and transient climate response to greenhouse gas concentrations (Seinfeld et al., 2016, IPCC 2013).

Only a fraction of aerosol can affect clouds; those aerosols that can activate to form cloud droplets (termed cloud condensation nuclei, CCN) must satisfy a certain range of physical size and chemical composition for the levels of water vapor supersaturation that develop in cloud-forming air parcels (Köhler, 1936; Seinfeld and Pandis, 2006). The properties and dynamical development of warm and mixed-phase clouds are sensitive to the number of cloud droplets formed. It is now established that anthropogenic emissions have strongly modulated global CCN and droplet number since the industrial revolution (e.g., Boucher et al., 2013; Raatikainen et al., 2013). Much work remains, however, to reduce the uncertainty associated with this forcing on climate (e.g., Seinfeld et al., 2016).

Appropriately capturing the variability in droplet number, and its sensitivity to aerosol (which is at the heart of aerosol-cloud interactions) requires a good description of aerosol size distribution and hygroscopicity (e.g., Fanourgakis et al., 2019), especially in boundary-layer clouds where liquid clouds and their radiative cooling dominates. Key

84 towards achieving this goal is to capture the source characteristics of major aerosol types,

85 and their chemical/microphysical evolution throughout their atmospheric residence.

86 Biomass burning (BB) aerosol has emerged as a major source of regional and global

87 aerosol, contributing up to 64% of global surface CCN concentrations (Spracklen et al.,

88 2011). The influence of BB is expected to increase in importance as the combustion of

89 biomass (natural and anthropogenic) is expected to accelerate in the future, especially in

90 Africa, while anthropogenic emissions decrease (Bond, et al. 2013, Andela et al., 2017).

91   Almost one third of annual global biomass burning emissions originate from

92 regional fires across the savannah and woodlands of sub-Saharan Africa, and one fourth

93 originate from southern Africa (van der Werf et al., 2010). From approximately June until

94 October, these intense BB emissions are subsequently transported over the southeast

95 Atlantic (SEA) region (Adebiyi and Zuidema, 2016; Garstang et al., 1996), greatly

96 elevating CCN levels above background concentrations (Ross, et al., 2003) and

97 interacting with low-level marine boundary layer clouds that are abundant in the SEA

98 (e.g., Seager et al., 2003; Grosvenor et al., 2018; Zuidema et al., 2018). The SEA

99 experiences a structure transition from marine stratocumulus to trade wind cumulus

100 clouds, so the coincidence of large BB aerosol plumes implies a potentially large role for

101 aerosol-cloud interactions to affect cloud radiative properties over a globally-relevant

102 system, potentially modulating the extent of each regime and the transition itself

103 (Yamaguchi et al., 2015; Zhou et al., 2017). The microphysical influence of BB aerosol

104 on clouds, however, is non-linear, as increasing aerosol levels enhance the competition of

105 CCN for water vapor, to the point where droplet formation may be insensitive to CCN

106 concentration level (e.g., Rissman et al., 2004; Ruetter et al., 2009; Bougiatioti, et al.,

107 2016). Dynamical adjustments (primarily vertical velocity) may also respond to CCN and

108 cloud droplet number changes - therefore it is important to quantify all these links, as

109 model-assessments of BB aerosol-cloud-climate interactions in the SEA critically rely on

110 them. Constraints, however, on such links are virtually nonexistent for this region of the

111 globe.

112   This study analyzes data collected in August 2017 on the NASA ObseRvations of

113 Aerosols above CLouds and their intEractionS (ORACLES) campaign, and provides a

114 systematic mapping of CCN concentration, aerosol size distribution, hygroscopicity, and

115 cloud vertical velocity in the SEA. The in-situ measurements are then coupled with a

116 state-of-the-art droplet parameterization to determine the in-cloud maximum

117 supersaturation (S_{max}) achieved in the cloud updrafts and its response to aerosol changes.

118 The data then is used to quantify the sensitivity of droplet formation to variations in

119 vertical velocity and aerosol. We also explore whether the presence of BB aerosol

120 correlates with shifts in the cloud vertical velocity driving droplet formation. These

121 perturbations in BB aerosol availability, linked with vertical updraft dynamics, and

122 predicted cloud droplet formation allow for understanding the drivers of droplet

123 formation in the SEA cloud deck, and the degree to which BB influences droplet

124 formation in the boundary layer.

125

126 **2.**   **Methods**

127 **2.1**   **Observational Data Set**

128   A complete description and overview of the project is provided by Redemann, et

129 al. (in preparation). All measurements were taken aboard the National Aeronautics and

130   Space Administration (NASA) P-3B aircraft from August 12th through 31st as part of the

131   ORACLES 2017 campaign. The aircraft was based at the International Airport

132   (0.3778°N, 6.7131°E) of São Tomé, an island off the west coast of central Africa. A map

133   of MODIS satellite fires for the month of August 2017 can be found in Figure 1. The

134   burning area is largely savanna grassland and the subsequent smoke plume travels

135   westward over the SEA region. This work focuses on data collected on eight different

136   research flights in the 2017 campaign during which instrumentation providing all relevant

137   aerosol microphysical and cloud-scale dynamics data performed optimally. Flight paths

138   for all data used in this work can be found in Figure 1. Most flights followed a "routine"

139   route going out to 5°E longitude and then due South. Each flight included legs at varying

140   altitudes to capture the characteristics of the plume, the marine boundary layer (MBL),

141   and the cloud deck. This work primarily focuses on the aerosol measured below-cloud in

142   the MBL, as that is the aerosol that will participate in cloud droplet activation.

143   **2.2   Instrumentation**

144   A summary of the relevant measurements obtained at each flight can be found in

145   Table 1. A solid diffuser inlet, characterized previously as having a 4μm dry diameter

146   cut-off (McNaughton, et al. 2007), was used to sample aerosol onboard the aircraft. A

147   Droplet Measurement Technologies (DMT; CCN-100) Continuous Flow Streamwise

148   Thermal Gradient Chamber (CFSTGC; Roberts and Nenes, 2005) was used to measure

149   CCN concentrations using a DMT constant pressure inlet operated at 600 mbar pressure.

150   Since CCN measurements are highly sensitive to fluctuations in pressure and their effect

151   on generated supersaturation (Raatikainen, et al. 2014), a flow orifice and active control

152   system were used upstream of the instrument to ensure that the pressure remained

153 constant, despite fluctuations in ambient pressure with altitude. The instrument was

154 operated in both "standard" mode, where supersaturation (SS%) was stepped between

155 0.1, 0.2, and 0.3% by changing the temperature gradient in the droplet growth chamber,

156 and in "scanning flow CCN analysis" (SFCA) mode (Moore and Nenes, 2009), where

157 supersaturation was varied from 0.1% to 0.4% by cycling the flow in a sinusoidal pattern

158 from 300 to 1000 cm^3 min^{-1} while maintaining a constant temperature gradient in the

159 growth chamber. Aerosol particles that activated into droplets sized greater than 0.5μm

160 were then counted as CCN by the optical particle counter located at the exit of the

161 CFSTGC growth chamber.

162 A DMT Ultra High Sensitivity Aerosol Spectrometer (UHSAS) was also operated

163 on the same 600mbar constant pressure inlet as the CFSTGC to detect the aerosol

164 concentration from 80 to 1000 nm (Table 1). Comparison of UHSAS with DMA

165 distributions revealed that the UHSAS counting efficiency dropped below about 80 nm

166 (Howell et al., in preparation), which should not strongly affect our subsequent analysis –

167 as particles larger than 80nm diameter contribute the exclusive majority of CCN that

168 activate into droplets for the conditions considered. The aerosol size distribution was

169 combined with CCN measurements to calculate the hygroscopicity parameter, κ, of the

170 observed aerosol (Petters and Kreidenweis, 2007), following a procedure adopted in

171 numerous studies (e.g., Kalkavouras et al., 2019; Bougiatioti et al., 2016; Moore et al.,

172 2011; Lathem et al., 2013) where integration of the particle size distribution from the

173 largest resolved bin in the UHSAS down to a characteristic size, d_{crit} (also known as the

174 "critical diameter"), matches the measured CCN concentration. The hygroscopicity then

175   is obtained from from d_{crit} and the instrument supersaturation, following Kalkavouras et

176   al. (2019).

177   Vertical winds on the P-3B were measured with the Turbulent Air Motion

178   Measurement System (TAMMS) (Thornhill et al., 2003). Fast-response flow-angle,

179   pressure, and temperature sensors combined with a GPS corrected inertial navigation

180   system (INS) provide 50 Hz inputs to compute 20 Hz averaged vertical winds via the full

181   air motion equations from Lenschow (1986). The updraft velocities are then used as an

182   input to calculate cloud droplet number concentration via a Gaussian distribution of

183   updraft velocities (Section 2.3).

184   An Aerodyne High-Resolution Time-of-Flight Aerosol Mass Spectrometer (HR-

185   ToF-AMS) (DeCarlo, et al., 2006) was used to monitor bulk chemical composition of

186   sampled aerosol throughout all flights. The bulk chemical composition acquired is then

187   used to calculate the "bulk" κ (Petters and Kreidenweis, 2007), based on the mass

188   fraction of organics and sulfate in the aerosol – assuming that the hygroscopicity of the

189   organic fraction, κ_{org}=0.1, and of sulfate, $\kappa_{sulfate}$=0.6. We have also ignored the effects of

190   insoluble material – such as black carbon – as it constitutes a small volume fraction of the

191   aerosol and has a negligible influence on hygroscopicity. The bulk-derived κ allows for

192   comparison with the directly calculated κ from the CFSTGC and UHSAS measurements,

193   even if the AMS-derived values correspond to larger sizes than the CCN-derived κ.

194   Nevertheless, strong agreement is found between the two κ values (Table 1; Figure S1),

195   thus confirming that the internal mixture assumption inherent to CCN-derived

196   hygroscopicity applies, and, that the composition varies little over the size range between

197   d_{crit} (~100-200nm) and the peak of the mass distribution resolved by the AMS. It should

198 also be noted that all of the AMS data was in high-sensitivity mode; the AMS heater was

199 operated at an indicated 600 ºC, which was tested and proved optimal for the ORACLES

200 BB Organic Aerosol plume. The data were processed using the standard AMS software

201 (Squirrel, version 1.41).

202   A Droplet Measurement Technologies (DMT) Cloud Droplet Probe (CDP) was

203 used to measure the cloud droplet number from 2 to 50 micron in diameter. The CDP was

204 modified according to Lance et al. (2010) to reduce coincidence problems. The total

205 cloud droplet number (N_d) from the CDP is compared against the predicted N_d from the

206 cloud droplet parameterization. These comparisons are done in flights with mostly

207 stacked legs in the MBL and clouds; occasionally, flights where aerosol and cloud were

208 immediately before or after each other were used (but not stacked).

209 **2.3   Predicted Cloud Droplet Number**

210   The droplet activation process is the direct microphysical link between clouds and

211 aerosol. Every aerosol particle, to activate and form a cloud droplet, requires exposure to

212 a "critical" supersaturation (or above) for enough time to grow past a "critical" wet size

213 (Nenes et al., 2001) that ensures unconstrained growth. Applying this principle to

214 ambient clouds is confounded by the complex relationship of supersaturation with aerosol

215 size distribution, hygroscopicity, and the characteristic vertical updraft velocity. State-of-

216 the-art cloud droplet parameterizations (e.g., Ghan et al., 2011; Morales and Nenes,

217 2014), however, resolve this relation and determine the cloud droplet number (N_d),

218 maximum available supersaturation (S_{max}), and sensitivity of N_d to changes in aerosol

219 concentration (N_a), vertical updraft velocity (w), and CCN activity (κ).

220   In this study, we utilize the Nenes and Seinfeld (2003) parameterization with

221   improvements introduced by Fountoukis and Nenes (2005), Barahona et al., (2010) and

222   Morales and Nenes (2014). In applying the droplet parameterization, we integrate over

223   the distribution of vertical velocities within the boundary layer – by utilizing the

224   "characteristic vertical velocity" approach of Morales and Nenes (2010). In this

225   approach, instead of numerically integrating over a probability density distribution

226   (PDF), the parameterization is applied at a "characteristic" velocity, w^*, that yields the

227   same result as the integrated value over the PDF. To derive w^*, the measured updrafts

228   (positive vertical winds), w, are taken from all segments just below cloud in a given

229   flight, then fit to a Gaussian distribution with zero mean; $w^*=0.79\sigma_w$, where σ_w is the

230   width of the vertical velocity spectrum (Morales and Nenes, 2010). Stratocumulus clouds,

231   such as those sampled in this study, are well characterized by a Gaussian distribution of

232   vertical velocities with a mean close to zero (Morales and Nenes, 2010). A comparison

233   between the predicted N_d from the parameterization and the measured N_d from the CDP

234   can be found in Figure S2. The parameterized N_d was, on average, within 20% of the

235   measured N_d, which is within the difference range of previous droplet closure studies

236   (e.g., Meskhidze et al., 2005; Fountoukis et al., 2007; Morales et al., 2011).

237

238   **3.   Results and Discussion**

239   **3.1   Marine Boundary Layer Air Mass Characterization**

240   Characteristic vertical profiles of CCN concentrations from 0.1 to 0.4%

241   supersaturation for flights used in this work are shown in Figure 2. Earlier flights (RF01 –

242   RF03) have lower BB plume heights, relatively little vertical variation of concentration

243   within the plume, and high CCN concentrations in the marine boundary layer (MBL).

244   Later flights (RF08 – RF12) show distinct layering in the plume, a higher plume cap

245   altitude, and lower MBL concentrations. Hereon we focus on aerosol concentrations in

246   the MBL, being the relevant aerosol providing CCN for BL cloud formation. A summary

247   of the MBL aerosol concentrations, CCN–derived κ (averaged over all the

248   supersaturations measured), and characteristic vertical updraft velocity (w^*) is provided

249   for all flights in Table 1. Flights are classified according to the observed MBL aerosol

250   concentrations from the UHSAS into categories defined, for the purposes of this work, as

251   *"polluted"* (exceeding 800 cm^{-3}), *"intermediate"* (500-800 cm^{-3}), and *"clean"* (below

252   500 cm^{-3}). MBL aerosol concentration is higher earlier on in August and decreases as the

253   mission progresses. The average CCN-derived κ for the MBL aerosol is fairly consistent,

254   ranging from 0.2 to 0.4, and agrees well with the κ estimated from the bulk MBL aerosol

255   elemental composition as measured by the aerosol mass spectrometer, implying that the

256   aerosol is chemically uniform throughout the ultrafine aerosol size range (Figure S1).

257   Characteristic vertical updrafts are higher earlier in August, averaging 0.4 ms^{-1},

258   and decrease to around 0.3 ms^{-1} later in the campaign. A decrease in MBL aerosol

259   concentration is also seen during this time, with earlier flights seeing aerosol

260   concentrations reaching up to 1000 cm^{-3} and later decreasing to 200 cm^{-3}. The average

261   BB plume aerosol concentrations aloft range from around 1250 cm^{-3} to 3000 cm^{-3}, but

262   show no distinct trends throughout the month. However, an interesting trend can be found

263   in comparing the altitudes of the bottom of the BB plume and the top of the MBL cloud

264   deck with the characteristic vertical updraft velocities – a lower w^* of 0.3 ms^{-1} coincides

265   with observation of a clean, low-aerosol "gap" between the top of the MBL clouds and

266   the bottom of the BB plume. In higher w^* flights (0.4 ms^{-1}), the BB plume extends all the

267   way down to the top of the MBL cloud layers. In these flights, the BB plume is observed

268   to have one single, well-mixed layer throughout, while the later flights ($w^* \sim 0.3$ ms^{-1}) are

269   characterized by two distinct layers in the plume.

270

271   **3.2   Predicted Droplet Number and Maximum Supersaturation**

272   Figure 3a presents predicted droplet number (N_d) and CCN (at 0.1%

273   supersaturation) as a function of total aerosol concentration (N_a) for the marine boundary

274   layer (MBL) legs of all flights. Above an aerosol concentration of ~600 cm^{-3}, droplet

275   number concentration becomes progressively less responsive to further increases in CCN

276   number (as the incremental change in N_d is less as   CCN increases) and becomes

277   effectively insensitive ($\partial N_d / \partial N_a \sim 0$) for an aerosol concentration exceeding ~1000 cm^{-3}.

278   The reason behind this increasing insensitivity can be seen in Figure 3b, which presents

279   N_d against N_a for all the MBL leg data; the data are colored by supersaturation. For low

280   values of N_a and N_d (~200cm^{-3}), S_{max} tends to be high (just over 0.2%) and the response

281   of N_d to increases in aerosol is strong. However, when transitioning from "clean" to

282   "intermediate" MBL conditions, N_d is less sensitive to increases in aerosol, because S_{max}

283   decreases, and mitigates some of the expected droplet number response. Upon reaching

284   "polluted" conditions (>800 cm^{-3}), the decrease in S_{max} is even stronger, entering into a

285   regime where any additional aerosol can no longer substantially augment cloud droplets,

286   owing to the extreme competition of the high CCN concentrations for water vapor. This

287   water vapor-limited regime occurs when the S_{max} is less than 0.1% (Figure 3b); given that

288   water vapor availability is generated through expansion cooling in updrafts, this type of

289   limitation is also known as the "updraft-limited" regime of droplet formation (Ruetter et

290   al., 2009).

291

292   **3.3   Droplet Number Sensitivity**

293   The previous section pointed out the variable sensitivity of droplet number to

294   aerosol perturbations, depending on the conditions of cloud formation. To further explore

295   such issues, we explicitly calculate the sensitivities (partial derivatives) of droplet number

296   in the MBL to changes in aerosol number, characteristic vertical updraft velocity, and

297   CCN activity, computed by the parameterization using a finite difference approximation.

298   This is shown in Figure 4 for $\partial N_d/\partial N_a$ (top panel), $\partial N_d/\partial w$ (middle panel) and $\partial N_d/\partial \kappa$

299   (bottom panel). Results are shown for three flights, corresponding to each pollution class

300   of Table 1: "polluted" (RF02), "intermediate" (RF09), and "clean" (RF10). Sensitivity of

301   droplet number to total aerosol concentration ($\partial N_d/\partial N_a$) is fairly comparable between the

302   two lower concentration conditions and approaches insensitivity ($\partial N_d/\partial dN_a < 0.1$) when

303   the total aerosol concentration exceeds 1000 cm^{-3}. Maximum in-cloud supersaturation

304   decreases steadily as N_a increases and $\partial N_d/\partial dN_a$ appreciably decreases when S_{max} drops

305   below 0.12% (Figure 4, top panel).

306   As $\partial N_d/\partial N_a$ decreases with increasing levels of aerosol, droplet sensitivity to

307   vertical updraft velocity, $\partial N_d/\partial w$, becomes increasingly important and completely

308   dominates droplet variability for high aerosol numbers. The reason why droplets become

309   so sensitive to vertical velocity fluctuations under polluted conditions, is because vertical

310   velocity drives supersaturation generation; at low supersaturation, when there is very

311   strong competition for water vapor from the many CCN present ("velocity-limited

312 regime"), any increase in vertical velocity augments supersaturation and droplet number.

313 For low CCN concentrations, however, supersaturation is high so that fluctuations in

314 aerosol translate to an almost equal response in droplet number ($\partial N_d/\partial dN_a \sim 1$; Figure 4,

315 top panel), therefore fluctuations in vertical velocity, hence supersaturation, do not affect

316 droplet number ($\partial N_d/\partial w$ small). The low MBL aerosol concentrations lead to the highest

317 sensitivity of N_d to N_a (approaching 100%), creating an "aerosol-limited" condition where

318 there is sufficient available supersaturation to activate virtually every aerosol added to the

319 MBL layer. A ~5x increase in N_a leads to a ~50% decrease in the sensitivity of N_d to N_a

320 to around 40%, with the highest aerosol values corresponding to even lower sensitivities

321 to aerosol number, approaching below 10% and clearly behavior consistent with a

322 "velocity-limited" regime.

323   Predicted droplet sensitivity to κ displays a unique trend (Figure 4, bottom panel),

324 becoming stronger initially with increasing aerosol, peaking at intermediate

325 concentrations and then rapidly dropping towards insensitivity, when supersaturation

326 approaches 0.1%. This sudden insensitivity to CCN activity aligns with the clouds being

327 overseeded when supersaturation is starting to be depleted – once supersaturation is not

328 as readily available, any characteristics of the aerosol cease to play a strong role in

329 activation. However, prior to reaching the point of being insensitive to aerosol, increased

330 sensitivity to κ is opposite to the expected trend from N_a – indicating that the fluctuation

331 in chemical composition, when droplet formation is in a "competitive" regime (Figure

332 4c), may be an important contributor to droplet formation – consistent with the findings

333 of Bougiatioti et al., (2017) for droplet formation in an urban environment in the E.

334 Mediterranean. We emphasize here that the sensitivity to κ (Figure 4c) is not from its

335 changes over size (which we show above to be small), but rather changes over space and

336 time.

337

338 **3.2.1 Impact of Boundary Layer Turbulence**

339 Throughout the entirety of flights, the maximum predicted droplet number

340 reaches a plateau, where additional aerosol does not result in any significant increase in

341 N_d. An example of this behavior is presented in Supplementary Figure S4 (where data of

342 calculated N_d is presented for the entire research flight, as opposed to only the segments

343 in the MBL shown in previous sections). This plateau, owing to the development of

344 strong water vapor limitations, is termed limiting droplet number, N_d^{lim}, and should

345 largely be a function of vertical velocity – precisely because we are in a velocity-limited

346 regime. This realization implies that much of the droplet number variability (measured or

347 retrieved) in clouds strongly influenced by BB plumes reflects the underlying shifts in

348 cloud dynamics associated with each concentration "regime". Indeed, the characteristic

349 velocity in the MBL tends to increase as the MBL clouds become progressively polluted

350 (Figure 5); the higher pollution flights (RF01 and RF02) all fall in mid-August and are

351 coincident with a higher characteristic vertical updraft velocity of ~ 0.4, while "clean"

352 MBL flights coincide with lower vertical updraft velocity values of ~0.3 and occur

353 towards the end of August. "Intermediate" scenario flights are divided between the two

354 characteristic vertical updraft velocities observed. When the flight-specific characteristic

355 velocity is then used to calculate the droplet response, it follows a trend with aerosol

356 levels that magnifies droplet response from what is expected by increasingly adding

357 pollution alone. In contrast, the aerosol concentration above the MBL is inversely

358   correlated with w^* (Figure 5), possibly a result of enhanced mixing between the MBL and

359   the free troposphere (rich in BB aerosol) that is associated with the elevated levels of

360   turbulence (w^*).

361   The impact of increased w^* on the droplet number is shown for "polluted",

362   "intermediate" and "clean" conditions in the inset plot of Figure 6 – which shows N_d^{lim}

363   for each concentration class for w^* between 0.1 and 0.6 ms^{-1}. For polluted conditions,

364   transitioning from 0.3 to 0.4 ms^{-1} increases droplet number from 400 to 500 cm^{-3}, which

365   is a 20-25% increase. The enhancement is equally important for intermediate and clean

366   conditions (although less in absolute number), and always comparable to droplet

367   enhancements from changes in BB concentration.

368

369   **3.4   Water-vapor limitations and the lifetime of BB aerosol in the MBL**

370   Above an aerosol concentration of ~800 cm^{-3} when water vapor availability is

371   severely limited, N_d no longer increases in response to increases in CCN (Figure 3a). An

372   important consequence is that under such conditions, much of the BBOA does not

373   activate into cloud droplets and is therefore not lost through wet deposition. Because of

374   this, the degree of water vapor competition (and supersaturation level) is directly related

375   to BB lifetime in the MBL. $\partial N_d/\partial dN_a$ may then be inversely linked to CCN lifetime,

376   where "velocity-limited" conditions, characterized by the smallest droplet activation

377   fraction and $\partial N_d/\partial dN_a$, also have the largest lifetime and vice versa for "clean" MBL

378   conditions.

379

380

381 **4.   Implications and Conclusions**

382   BB aerosol levels in the SEA varied considerably throughout the 2017 ORACLES

383 deployment. Earlier in the campaign, high aerosol concentrations were observed in the

384 MBL (800-1000 cm^{-3}), which decreased mid-campaign to concentrations between 500-

385 800 cm^{-3}, and in late August and early September, relatively clean MBL conditions were

386 seen (<500 cm^{-3}). On 12-13 August, MBL aerosol concentrations exceeded 1000 cm^{-3}.

387 From the observed aerosol size distribution and CCN concentrations, we constrained the

388 aerosol hygroscopicity – which was in agreement with estimates from bulk chemical

389 composition measurements; together with observed MBL vertical velocity distributions,

390 we then calculate droplet number concentrations using a state-of-the-art droplet activation

391 parameterization. Droplet closure was achieved within 20%, consistent with the degree of

392 closure achieved in past studies.

393   From the analysis of the dataset, when aerosol concentrations exceed ~900 cm^{-3}

394 and maximum supersaturation approaches 0.1%, droplet formation in the MBL begins to

395 enter a "velocity-limited" droplet activation regime, where cloud droplet number

396 responds weakly to CCN concentration increases. Lower MBL concentrations (500 cm^{-3}

397 or less) were observed later in the campaign (late August to early September), thus

398 leading to a much higher predicted S_{max} of 0.2%, and much higher fraction of activated

399 CCN. Under clean conditions, vertical velocity generates ample supersaturation, so

400 droplet formation is limited by the number of aerosol particles in the MBL. Overall this

401 leads to a buffering of the N_d response to aerosol, so that N_d variability is much less

402 (down to 1/10 or less) than that seen for the underlying CCN.

403   Droplet formation sensitivity to aerosol concentration, vertical updraft velocity,

404   and the hygroscopicity parameter, κ, vary and contribute to the total droplet response in

405   the MBL clouds. Droplet sensitivity to vertical velocity increases an order of magnitude

406   as aerosol concentration reaches 1000 cm^{-3}. This highlights the increased (and eventually

407   dominant) role that vertical velocity plays in droplet formation in a "polluted" MBL

408   environment. Below ~500 cm^{-3}, in a "clean" MBL, droplet formation is much more

409   sensitive to changes in aerosol concentration than to the observed changes in vertical

410   updrafts. In the "competitive" regime, where the MBL has "intermediate" pollution (500-

411   800 cm^{-3}), hygroscopicity (κ) variations emerges as an important driver of droplet number

412   variability, which is something not seen for either "clean" or "polluted" MBL conditions.

413   Throughout the month of August, a shift is observed in w^*, from ~0.45 m s^{-1} down to

414   ~0.26 m s^{-1}, which affects the maximum droplet number that can be generated in the

415   MBL. $N_d{}^{lim}$ is significantly affected by changes in w^*, especially in higher MBL pollution

416   conditions, where the effects of increased characteristic vertical updraft velocity

417   significantly magnifies droplet number concentrations compared to trends seen in

418   "intermediate" and "clean" MBL environments.

419   Identifying regimes where droplet number variability is primarily driven by

420   updraft velocity changes, and not aerosol concentration, is key for interpreting aerosol

421   indirect effects. This is particularly important when using remote sensing data, as can be

422   seen from the data here: diagnosing aerosol indirect effects using above-cloud aerosol

423   would give opposite trends from what actually occurs in the MBL – because BB plume

424   aerosol decreases as the MBL aerosol increases. Nevertheless, the correlations here

425   between above-cloud and MBL aerosol level might be a useful way to diagnose MBL

426   aerosol – from which N_d can eventually be determined. Furthermore, when droplet

427   number is in the velocity-limited regime, N_d responds proportionally to changes in w^*,

428   offering the possibility of remote sensing of w^* under these specific conditions (specific

429   criteria need to be developed to help define when velocity-limited conditions occur, e.g.,

430   combining collocated in-situ and remote sensing data from field intensives).

431   Very interesting are the trends observed between MBL dynamics, height and the

432   aerosol levels in the MBL and the BB plume. w^* is higher earlier in August and decreases

433   later in the campaign; MBL aerosol concentration correlates with w^*, while an inverse

434   correlation is seen for the aerosol in the BB plume above the MBL. A similarly

435   interesting trend can be found between w^*, the base altitude of the BB plume and the top

436   of the MBL cloud deck: higher w^* corresponds to a BB plume that extends down to the

437   top of the MBL cloud layers, while lower w^* is characterized by two distinct layers in the

438   plume. Although what drives these correlations is not fully understood, it is likely related

439   to the seasonality of the MBL height and its role in regulating mixing between the MBL

440   and aloft (also discussed in Zhang et al., 2019). Indeed, the atmosphere is likely less

441   stable in August, encouraging buoyant parcels (hence larger w^*) than in September. w^*

442   enhancement may also result from enhanced cloud-top radiative cooling driven by LWC

443   changes between the early and later flights of the campaign – the nearly threefold

444   increase in cloud droplet number and the expected LWC response, however, suggests that

445   clouds may actually be thinner (Painemal and Zuidema, 2010; Wood et al., 2012; de

446   Szoeke et al., 2018). Water vapor in the FT, which is strongly correlated with smoke

447   occurrence in the FT, would also reduce the longwave emission from the top of the

448   stratocumulus and thereby reduce the turbulent driving of the PBL. Water vapor in the

449   outflow layers is driven by the proximity of the continental PBL to the warm continental

450   surface with enhanced evaporation – and is not related to aerosol processes. Absorption

451   of solar radiation from black carbon in the MBL may also suppress turbulence and w^*

452   (Wilcox et al., 2016), although our data suggests these effects may not be strong enough

453   to reverse the trend imposed by any MBL seasonality. A thorough attribution of the link

454   between w^*, aerosol, MBL structure and the large scale remains to be carried out, though

455   results here suggest simple thresholds on these variables could help models determine

456   how to treat droplet activation in different scenarios.

457   Although BB aerosol variations can profoundly impact cloud microphysical

458   characteristics, concurrent variations in vertical velocity must also be considered to fully

459   understand the drivers of droplet variability, especially when used to evaluate models and

460   estimates of aerosol-cloud-climate interactions. The small activation fraction of aerosols

461   under polluted MBL conditions may promote the persistence of aerosol for longer in the

462   MBL, extending the reach and influence of BB aerosol in the SEA.

463

Acknowledgements

MK and AN gratefully acknowledge funding from NASA ORACLES grant NNX15AL68G and the European Research Council, CoG-2016 project PyroTRACH (726165) funded by H2020-EU.1.1. – Excellent Science. All other authors acknowledge support from the NASA EVS-2 program for their individual ORACLES grants. All ORACLES datasets are publicly available through doi: 10.5067/Suborbital/ORACLES/P3/2017_V1

Code/Data availability

The droplet parameterization used for the calculations in the study is available from the athanasios.nenes@epfl.ch upon request. ORACLES mission data can be downloaded from http://espoarchive.nasa.gov/archive/browse/oracles.

Author contribution

Conceptualization, M.K. and A.N.; methodology, M.K. and A.N.; software, A.N.; formal analysis, M.K., A.N., S.H.; investigation, M.K. and A.N.; writing—original draft preparation, M.K. and A.N.; writing—review and editing: all authors.

Competing interests

The authors declare no competing interests.

References

Adebiyi, A. A., and Zuidema, P.: The role of the southern African easterly jet in modifying the southeast Atlantic aerosol and cloud environments, *Q.J.R. Meteorol. Soc.*, 142, 1574-1589. doi:10.1002/qj.2765, 2016.

Albrecht, B. A.: Aerosols, Cloud Microphysics, and Fractional Cloudiness, *Science*, 245, 4923, 1227-1230, doi:10.1126/science.245.4923.1227, 1989.

Andela, N., Morton, D. C., Giglio, L., Chen, Y., van der Werf, G. R., Kasibhatla, P. S., DeFries, R. S., Collatz, G. J., Hantson, S., Kloster, S., Bachelet, D., Forrest, M., Lasslop, G., Li, F., Mangeon, S., Melton, J. R., Yue, C., Randerson, J. T.: A human-driven decline in global burned area, *Science*, 356, 6345, 1356-1362, doi: 10.1126/science.aal4108, 2017.

Barahona, D., West, R. E. L., Stier, P., Romakkaniemi, S., Kokkola, H., and Nenes, A.: Comprehensively accounting for the effect of giant CCN in cloud activation parameterizations, *Atmos. Chem. Phys.,* 10, 2467-2473, https://doi.org/10.5194/acp-10-2467-2010, 2010.

Bond, T. C., Doherty, S. J., Fahey, D. W., Forster, P. M., Berntsen, T., DeAngelo, B. J., Flanner, M. G., Ghan, S., Kärcher, B., Koch, D., Kinne, S., Kondo, Y., Quinn, P. K., Sarofim, M. C., Schultz, M. G., Schulz, M., Venkataraman, C., Zhang, H., Zhang, S., Bellouin, N., Guttikunda, S. K., Hopke, P. K., Jacobson, M. Z., Kaiser, J. W., Klimont, Z., Lohmann, U., Schwarz, J. P., Shindell, D., Storelvmo, T., Warren, S. G., Zender, C. S.: Bounding the role of black carbon in the climate system: A scientific assessment, *J. Geophys. Res.*, 118, 5380– 5552, doi:10.1002/jgrd.50171, 2013.

Boucher, O., Randall, D., Artaxo, P., Bretherton, C., Feingold, G., Forster, P., Kerminen, V.-M., Kondo, Y., Liao, H., Lohmann, U., Rasch, P., Satheesh, S. K., Sherwood, S., Stevens, B., and Zhang, X. Y.: Clouds and aerosols. In *Climate Change 2013: The Physical Science Basis. Contribution of Working Group I to the Fifth Assessment Report of the Intergovernmental Panel on Climate Change.* T.F. Stocker, D. Qin, G.-K. Plattner, M. Tignor, S.K. Allen, J. Doschung, A. Nauels, Y. Xia, V. Bex, and P.M. Midgley, Eds. Cambridge University Press, pp. 571-657, doi:10.1017/CBO9781107415324.016, 2013.

Bougiatioti, A., Bezantakos, S., Stavroulas, I., Kalivitis, N., Kokkalis, P., Biskos, G., Mihalopoulos, N., Papayannis, A., and Nenes, A.: Biomass-burning impact on CCN number, hygroscopicity and cloud formation during summertime in the eastern Mediterranean, *Atmos. Chem. Phys.*, 16, 7389-7409, doi:10.5194/acp-16-7389-2016, 2016.

Bougiatioti, A., Argyrouli, A., Solomos, S., Vratolis, S., Eleftheriadis, K., Papayannis, A., and Nenes, A.: CCN Activity, Variability and Influence on Droplet Formation during the HygrA-Cd Campaign in Athens. *Atmosphere*, 8, 108, 2017.

Cubison, M. J., Ervens, B., Feingold, G., Docherty, K. S., Ulbrich, I. M., Shields, L., Prather, K., Hering, S., and Jimenez, J. L.: The influence of chemical composition and

mixing state of Los Angeles urban aerosol on CCN number and cloud properties, *Atmos. Chem. Phys.*, 8, 5649-5667, doi:10.5194/acp-8-5649-2008, 2008.

DeCarlo, P.F., J.R. Kimmel, A. Trimborn, M.J. Northway, J.T. Jayne, A.C. Aiken, M. Gonin, K. Fuhrer, T. Horvath, K. Docherty, D.R. Worsnop, and J.L. Jimenez: Field-Deployable, High-Resolution, Time-of-Flight Aerosol Mass Spectrometer, Analytical Chemistry, 78: 8281-8289, 2006.

de Szoeke, S. P., Verlinden, K. L., and Covert, D.: Cloud-scale droplet number sensitivity to liquid water path in marine stratocumulus. *J.Geoph.Res*, 123, 5320–5334, doi: 10.1029/2017JD027508, 2018.

Dusek, U., Frank, G. P., Hildebrandt, L., Curtius, J., Schneider, J., Walter, S., Chand, D., Drewnick, F., Hings, S., Jung, D., Borrmann, S., and Andreae, M. O.: Size Matters More Than Chemistry for Cloud-Nucleating Ability of Aerosol Particles, *Science*, 312:578, 1375-1378, 2006.

Fanourgakis, G. S., Kanakidou, M., Nenes, A., Bauer, S. E., Bergman, T., Carslaw, K. S., Grini, A., Hamilton, D. S., Johnson, J. S., Karydis, V. A., Kirkevåg, A., Kodros, J. K., Lohmann, U., Luo, G., Makkonen, R., Matsui, H., Neubauer, D., Pierce, J. R., Schmale, J., Stier, P., Tsigaridis, K., van Noije, T., Wang, H., Watson-Parris, D., Westervelt, D. M., Yang, Y., Yoshioka, M., Daskalakis, N., Decesari, S., Gysel-Beer, M., Kalivitis, N., Liu, X., Mahowald, N. M., Myriokefalitakis, S., Schrödner, R., Sfakianaki, M., Tsimpidi, A. P., Wu, M., and Yu, F.: Evaluation of global simulations of aerosol particle and cloud condensation nuclei number, with implications for cloud droplet formation, *Atmos. Chem. Phys.*, 19, 8591-8617, https://doi.org/10.5194/acp-19-8591-2019, 2019.

Fountoukis, C., and Nenes, A.: Continued development of a cloud droplet formation parameterization for global climate models, *J. Geophys. Res.*, 110, D11212, doi:10.1029/2004JD005591, 2005.

Fountoukis, C., Nenes, A., Meskhidze, N., Bahreini, R., Brechtel, F., Conant, W. C., Jonsson, H., Murphy, S., Sorooshian, A., Varutbangkul, V., R. C. Flagan, and J. H. Seinfeld: Aerosol–cloud drop concentration closure for clouds sampled during ICARTT, *J.Geoph.Res.*, 112, D10S30, doi:10.1029/2006JD007272, 2007.

Garstang, M., Tyson, P. D., Swap, R., Edwards, M., Kållberg, P., and Lindesay, J. A.: Horizontal and vertical transport of air over southern Africa, *J. Geophys. Res.*, 101 (D19), 23721– 23736, doi:10.1029/95JD00844, 1996.

Ghan, S. J., Abdul-Razzak, H., Nenes, A., Ming, Y., Liu, X., Ovchinnikov, M., Shipway, B., Meskhidze, N., Xu, J., and Shi, X.: Droplet nucleation: Physically-based parameterizations and comparative evaluation*, J. Adv. Model. Earth Syst.*, 3, M10001, doi:10.1029/2011MS000074, 2011.

Grosvenor, D. P., Sourdeval, O.,Zuidema, P., Ackerman, A.,Alexandrov, M. D., Bennartz, R.,et al.: Remote sensing of droplet number concentration in warm clouds: A

559 review of the currentstate of knowledge and perspectives, *Rev.Geoph*, 56, 409–453,
560 doi:10.1029/2017RG000593, 2018.

561 Howell, et al., in prep.

562 IPCC, 2013: Climate Change 2013: The Physical Science Basis. Contribution of Working
563 Group I to the Fifth Assessment Report of the Intergovernmental Panel on Climate
564 Change [Stocker, T.F., D. Qin, G.-K. Plattner, M. Tignor, S.K. Allen, J. Boschung, A.
565 Nauels, Y. Xia, V. Bex and P.M. Midgley (eds.)]. Cambridge University Press,
566 Cambridge, United Kingdom and New York, NY, USA, 1535 pp,
567 doi:10.1017/CBO9781107415324.

568 Kalkavouras, P., Bougiatioti, A., Kalivitis, N., Tombrou, M., Nenes, A., and
569 Mihalopoulos, N.: Regional New Particle Formation as Modulators of Cloud
570 Condensation Nuclei and Cloud Droplet Number in the Eastern Mediterranean, *Atmos.*
571 *Chem. Phys.*, 19, 6185-6203, https://doi.org/10.5194/acp-19-6185-2019, 2019

572 Kanakidou, M., Seinfeld, J. H., Pandis, S. N., Barnes, I., Dentener, F. J., Facchini, M. C.,
573 Van Dingenen, R., Ervens, B., Nenes, A., Nielsen, C. J., Swietlicki, E., Putaud, J. P.,
574 Balkanski, Y., Fuzzi, S., Horth, J., Moortgat, G. K., Winterhalter, R., Myhre, C. E. L.,
575 Tsigaridis, K., Vignati, E., Stephanou, E. G., and Wilson, J.: Organic aerosol and global
576 climate modelling: a review, *Atmos. Chem. Phys.*, 5, 1053-1123, doi:10.5194/acp-5-
577 1053-2005, 2005.

578 Kerminen, V.-M., Paramonov, M., Anttila, T., Riipinen, I., Fountoukis, C., Korhonen, H.,
579 Asmi, E., Laakso, L., Lihavainen, H., Swietlicki, E., Svenningsson, B., Asmi, A., Pandis,
580 S. N., Kulmala, M., and Petäjä, T.: Cloud condensation nuclei production associated with
581 atmospheric nucleation: a synthesis based on existing literature and new results, *Atmos.*
582 *Chem. Phys.*, 12, 12037-12059, doi:10.5194/acp-12-12037-2012, 2012.

583 Klein, S. A., and Hartmann, D. L.: The Seasonal Cycle of Low Stratiform Clouds. *J.*
584 *Climate*, 6, 1587–1606, doi:10.1175/1520-0442(1993)006<1587:TSCOLS>2.0.CO;2,
585 1993.

586 Kohler, H.: The nucleus in and the growth of hygroscopic droplets, *Trans Farad Soc*, 32,
587 1152–1161, 1936.

588 Lance, S., Brock, C. A., Rogers, D., and Gordon, J. A.: Water droplet calibration of the
589 Cloud Droplet Probe (CDP) and in-flight performance in liquid, ice and mixed-phase
590 clouds during ARCPAC, Atmos. Meas. Tech., 3, 1683–1706,
591 https://doi.org/10.5194/amt-3-1683-2010, 2010.

592 Lathem, T.L., A.J. Beyersdorf, K.L. Thornhill, E.L. Winstead, M.J. Cubison, A.
593 Hecobian, J.L. Jimenez, R.J. Weber, B.E. Anderson, and Nenes, A.: Analysis of CCN
594 activity of Arctic aerosol and Canadian biomass burning during summer 2008,
595 *Atmos.Chem.Phys.*, 13, 2735-2756, 2013.

596 Lenschow, D.H., ed. 1986: *Probing the Atmospheric Boundary Layer*. Amer. Meteorol.
597 Soc.

598 McNaughton, C. S., Clarke, A. D., Howell, S. G., Pinkerton, M., Anderson, B., Thornhill,
599 L., Hudgins, C., Winstead, E., Dibb, J. E., Scheuer, E., and Maring, H.: Results from the
600 DC-8 Inlet Characterization Experiment (DICE): Airborne Versus Surface Sampling of
601 Mineral Dust and Sea Salt Aerosols, *Aero. Sci. Tech.*, 41:2, 136-159,
602 doi:10.1080/02786820601118406, 2007.

603 Meskhidze, N., Nenes, A., Conant, W. C., and Seinfeld, J.H.: Evaluation of a new Cloud
604 Droplet Activation Parameterization with In Situ Data from CRYSTAL-FACE and
605 CSTRIPE, *J.Geoph.Res.*, 110, D16202, doi:10.1029/2004JD005703, 2005.

606 Meyer, K., Platnick, S., and Zhang, Z.: Simultaneously inferring above-cloud absorbing
607 aerosol optical thickness and underlying liquid phase cloud optical and microphysical
608 properties using MODIS, J. Geophys. Res. Atmos., 120, 5524–5547,
609 doi:10.1002/2015JD023128, 2015.

610 Moore, R. H., and Nenes, A.: Scanning Flow CCN Analysis—A Method for Fast
611 Measurements of CCN Spectra, *Aero. Sci. Tech.*, 43:12, 1192-1207,
612 doi:10.1080/02786820903289780, 2009.

613 Moore, R.H., Bahreini, R., Brock, C.A., Froyd, K.D., Cozic, J., Holloway, J.S.,
614 Middlebrook, A.M., Murphy, D.M., Nenes, A.: Hygroscopicity and Composition of
615 Alaskan Arctic CCN During April 2008, *Atmos.Chem.Phys.*, 11, 11807-11825, 2011.

616 Morales, R., and Nenes, A.: Characteristic updrafts for computing distribution-averaged
617 cloud droplet number and stratocumulus cloud properties, *J. Geophys. Res.*, 115, D18220,
618 doi:10.1029/2009JD013233, 2010.

619 Morales, R., Nenes, A., Jonsson, H., Flagan, R.C. and J.H. Seinfeld: Evaluation of a
620 diabatic droplet activation parameterization using in-situ cloud data, *J.Geoph.Res.*, 116,
621 D15205, doi:10.1029/2010JD015324, 2011.

622 Morales Betancourt, R. and Nenes, A.: Understanding the contributions of aerosol
623 properties and parameterization discrepancies to droplet number variability in a global
624 climate model, *Atmos. Chem. Phys.*, 14, 4809-4826, doi:10.5194/acp-14-4809-2014,
625 2014.

626 Myhre, G., Samset, B. H., Schulz, M., Balkanski, Y., Bauer, S., Berntsen, T. K., Bian, H.,
627 Bellouin, N., Chin, M., Diehl, T., Easter, R. C., Feichter, J., Ghan, S. J., Hauglustaine, D.,
628 Iversen, T., Kinne, S., Kirkevåg, A., Lamarque, J.-F., Lin, G., Liu, X., Lund, M. T., Luo,
629 G., Ma, X., van Noije, T., Penner, J. E., Rasch, P. J., Ruiz, A., Seland, Ø., Skeie, R. B.,
630 Stier, P., Takemura, T., Tsigaridis, K., Wang, P., Wang, Z., Xu, L., Yu, H., Yu, F., Yoon,
631 J.-H., Zhang, K., Zhang, H., and Zhou, C.: Radiative forcing of the direct aerosol effect
632 from AeroCom Phase II simulations, *Atmos. Chem. Phys.*, 13, 1853-1877,
633 doi:10.5194/acp-13-1853-2013, 2013.

634 Nenes., A., Ghan, S., Abdul-Razzak, H., Chuang, P.Y., Seinfeld, J.H.: Kinetic
635 Limitations on Cloud Droplet Formation and Impact on Cloud Albedo, *Tellus*, *53B*, 133-
636 149, 2001

637 Nenes, A., and Seinfeld, J. H.: Parameterization of cloud droplet formation in global
638 climate models, *J. Geophys. Res.*, 108, 4415, doi:10.1029/2002JD002911, D14, 2003.

639 Petters, M. D. and Kreidenweis, S. M.: A single parameter representation of hygroscopic
640 growth and cloud condensation nucleus activity, *Atmos. Chem. Phys.*, 7, 1961-1971,
641 doi:10.5194/acp-7-1961-2007, 2007.

642 Petters, M. D. and Kreidenweis, S. M.: A single parameter representation of hygroscopic
643 growth and cloud condensation nucleus activity – Part 2: Including solubility, *Atmos.
644 Chem. Phys.*, 8, 6273-6279, doi:10.5194/acp-8-6273-2008, 2008.

645 Painemal, D. and Zuidema, P.: Microphysical variability in Southeast Pacific
646 stratocumulus clouds: Synoptic conditions and radiative response, Atmos. Chem. Phys.,
647 10, 6255-6269. doi:10.5194/acp-10-6255-2010, 2010.

648 Pósfai, M., Simonics, R., Li, J., Hobbs, P. V., and Busek, P. R.: Individual aerosol
649 particles from biomass burning in southern Africa: 1. Compositions and size distributions
650 of carbonaceous particles, *J. Geophys. Res.*, 108, 8483, doi:10.1029/2002JD002291, D13,
651 2003.

652 Raatikainen,T., Nenes,A., Seinfeld, J. H., Morales,R., Moore, R. H., Lathem, T. L.,
653 Lance, S., Padro, L. T., Lin, J. J., Cerully, K., Bougiatioti, A., Cozic, J., Ruehl, C.,
654 Chuang, P. Y., Anderson, B., Flagan, R.C., Jonsson, H., Mihalopoulos, N., and J. N.
655 Smith: Worldwide data sets constrain the water vapor uptake coefficient in cloud
656 formation, *Proc.Nat.Acad.Sci.*, doi: 10.1073/pnas.1219591110, 2013.

657 Raatikainen, T., Lin, J. J., Cerully, K. M., Lathem, T. L., Moore, R. H., and Nenes, A.:
658 CCN Data Interpretation Under Dynamic Operation Conditions, *Aero. Sci. Tech.*, 48:5,
659 552-561, doi:10.1080/02786826.2014.899429, 2014.

660 Redemann, J., et al.: An overview of the ORACLES (ObseRvations of Aerosols above
661 CLouds and their intEractionS) project: aerosol-cloud-radiation interactions in the
662 Southeast Atlantic basin, in preparation.

663 Rissman, T., Nenes, A., and Seinfeld, J. H.: Chemical amplification (or dampening) of
664 the Twomey effect: Conditions derived from droplet activation theory, *J. Atmos. Sci.*, 61,
665 919–930, 2004.

666 Reutter, P., Su, H., Trentmann, J., Simmel, M., Rose, D., Gunthe, S. S., Wernli, H.,
667 Andreae, M. O., and Pöschl, U.: Aerosol- and updraft-limited regimes of cloud droplet
668 formation: influence of particle number, size and hygroscopicity on the activation of
669 cloud condensation nuclei (CCN), *Atmos. Chem. Phys.*, 9, 7067-7080,
670 https://doi.org/10.5194/acp-9-7067-2009, 2009

671 Roberts, G. C., and Nenes, A.: A Continuous-Flow Streamwise Thermal-Gradient CCN
672 Chamber for Atmospheric Measurements, *Aero. Sci. Tech.*, 39:3, 206-221,
673 doi:10.1080/027868290913988, 2005.

674 Ross, K. E., Piketh, S. J., Bruintjes, R. T., Burger, R. P., Swap, R. J., and Annegarn, H.
675 J.: Spatial and seasonal variations in CCN distribution and the aerosol-CCN relationship
676 over southern Africa, *J. Geophys. Res.*, 108, 8481, doi:10.1029/2002JD002384, D13,
677 2003.

678 Seager, R., Murtugudde, R., Naik, N., Clement, A., Gordon, N., & Miller, J.: Air–Sea
679 Interaction and the Seasonal Cycle of the Subtropical Anticyclones. *J. Climate*, 16, 1948-
680 1966, 2003.

681 Seinfeld, J.H. and Pandis, S.N.: Atmospheric Chemistry and Physics: From Air Pollution
682 to Climate Change. 2nd Edition, John Wiley & Sons, New York, 2006.

683 Seinfeld, J. H., Bretherton, C., Carslaw, K. S., Coe, H., DeMott, P. J., Dunlea, E. J.,
684 Feingold, G., Ghan, S., Guenther, A. B., Kahn, R., Kraucunas, I., Kreidenweis, S. M.,
685 Molina, M. J., Nenes, A., Penner, J. E., Prather, K. A., Ramanathan, V., Ramaswamy, V.,
686 Rasch, P. J., Ravishankara, A. R., Rosenfeld, D., Stephens, G., and Wood, R.: Improving
687 our fundamental understanding of the role of aerosol−cloud interactions in the climate
688 system, *Proc.Nat.Acad.Sci.*, 113 (21) 5781-5790; doi:10.1073/pnas.1514043113, 2016.

689 Sinha, P., Hobbs, P. V., Yokelson, R. J., Bertschi, I. T., Blake, D. R., Simpson, I. J., and
690 Gao, S.: Emissions of trace gases and particles from savanna fires in southern Africa, *J.*
691 *Geophys. Res.*, 108, 8487, doi:10.1029/2002JD002325, D13, 2003.

692 Spracklen, D. V., Carslaw, K. S., Pöschl, U., Rap, A., and Forster, P. M.: Global cloud
693 condensation nuclei influenced by carbonaceous combustion aerosol, *Atmos. Chem.*
694 *Phys.*, 11, 9067-9087, doi:10.5194/acp-11-9067-2011, 2011.

695 Thornhill, K. L., Anderson, B. E., Barrick, J. D. W., Bagwell, D. R., Friesen, R., and
696 Lenschow, D.: Air motion intercomparison flights during Transport and Chemical
697 Evolution in the Pacific (TRACE-P)/ACE-ASIA. Journal of Geophysical Research. 108.
698 10.1029/2002JD003108, 2003.

699 Twomey, S.: Pollution and the Planetary Albedo, *Atmos. Env.*, 8, 1251-1256,
700 doi:10.1016/0004-6981(74)90004-3, 1974.

701 Twomey, S.: The Influence of Pollution on the Shortwave Albedo of Clouds, *J. Atmos.*
702 *Sci.*, 34, 1149–1152, doi:10.1175/1520-0469(1977)034<1149:TIOPOT>2.0.CO;2, 1977.

703 van der Werf, G. R., Randerson, J. T., Giglio, L., Collatz, G. J., Mu, M., Kasibhatla, P.
704 S., Morton, D. C., DeFries, R. S., Jin, Y., and van Leeuwen, T. T.: Global fire emissions
705 and the contribution of deforestation, savanna, forest, agricultural, and peat fires (1997–
706 2009), *Atmos. Chem. Phys.*, 10, 11707-11735, doi:10.5194/acp-10-11707-2010, 2010.

707   Wilcox, E. M., Thomas, R. M., Praveen, P. S., Pistone, K., Bender, F. A.-M., and
708   Ramanathan, V.: Black carbon suppresses atmospheric turbulence, Proc. Nat. Acad. Sci.,
709   113, 42, 11794-11799; DOI: 10.1073/pnas.1525746113, 2016.

710   Wood, R., Leon, D., Lebsock, M., Snider, J., and Clarke, A. D.: Precipitation driving of
711   droplet concentration variability in marine low clouds, J. Geophys. Res., 117, D19210,
712   doi:10.1029/2012JD018305, 2012.

713   Yamaguchi, T., G. Feingold, J. Kazil,and A. McComiskey, A.: Stratocumulus to cumulus
714   transition in the presence of elevated smoke layers, *Geoph. Res. Lett.*, 42, 10,478–
715   10,485,doi:10.1002/2015GL066544, 2015.

716   Zhang, J. and Zuidema, P.: The diurnal cycle of the smoky marine boundary layer
717   observed during August in the remote southeast Atlantic, Atmos. Chem. Phys., 19,
718   14493-14516, doi:acp-19-14493-2019, 2019.

719   Zhou, X. and Ackerman, A. S. and Fridlind, A. M. and Wood, R. and Kollias, P.: Impacts
720   of solar-absorbing aerosol layers on the transition of stratocumulus to trade cumulus
721   clouds, Atmos. Chem. Phys., 17, 20, 12725-12742, doi:10.5194/acp-17-12725-2017,
722   2017.
723
724   Zuidema, P., Sedlacek, A. J. III,Flynn, C., Springston, S.,Delgadillo, R., Zhang, J., et al.:
725   The Ascension Island boundary layer in the remote southeast Atlantic is often smoky.
726   *Geoph. Res. Lett.*, 45, 4456–4465, doi:10.1002/2017GL076926, 2018.
727

728 **Tables**

729 **Table 1:** Average marine boundary layer (MBL) aerosol concentrations from the

730 UHSAS, CCN activity derived from in-situ CCN measurements (κ_{CCN}) and bulk chemical

731 composition (κ_{AMS}), and characteristic vertical updraft velocity (w^*). Aerosol conditions

732 are classified for each flights as "polluted", "intermediate", or "clean" based on the MBL

733 aerosol concentration.

Flight Number	Date	Pollution Category	Aerosol Number (cm^{-3})	*CFSTGC Operation Mode*	κ_{CCNc}	κ_{AMS}	w^* (ms^{-1})
RF01	12 Aug 17	Polluted	707 ± 104	Both$^\$$	0.4	-	0.44
RF02	13 Aug 17	Polluted	1012 ± 98	Both$^\$$	0.4	0.4	0.40
RF03	15 Aug 17	Intermediate	481 ± 109	SFCA$^\wedge$	0.4	0.4	0.42
RF08	24 Aug 17	Intermediate	493 ± 40	Both$^\$$	0.3	0.4	0.32
RF09	26 Aug 17	Intermediate	433 ± 34	CF*	0.4	0.4	0.35
RF10	28 Aug 17	Clean	205 ± 21	CF*	0.3	-	0.33
RF11	30 Aug 17	Clean	278 ± 24	Both$^\$$	0.2	0.4	0.24
RF12	31 Aug 17	Clean	195 ± 21	CF*	0.4	0.4	0.3$^\#$

734 * CF: Constant Flow operation of the CCN instrument.

735 $^\wedge$ SFCA: Scanning Flow CCN Analysis operation of the CCN instrument.

736 $^\$$ Both operation modes (CF, SFCA) of the CCN instrument were used.

737 # w^*=0.3 ms^{-1} assumed when calculating droplet number. This value was selected based

738 on the pollution category and date, and the average of corresponding w^* determined from

739 RF10, RF11.

740

741

742

743 **Figures Captions**

744

745 **Figure 1:** Map of ORACLES 2017 research flights used in this work, together with

746 aerosol optical thickness (AOT) of the August 2017 plume (Meyer et al., 2015). The inset

747 provides MODIS imagery of savannah fires throughout August 2017. Most flights are in

748 close proximity to the "routine" flight path of due South along 5°E Longitude.

749

750 **Figure 2:** Vertical profiles (altitude in meters) of CCN concentration (cm^{-3}) from 0.1% to

751 0.4% supersaturation for all flights in this work.

752

753 **Figure 3:** a) Predicted droplet number (N_d; cm^{-3}) and measured CCN (cm^{-3}) at 0.1%

754 supersaturation as functions of marine boundary layer aerosol concentration (N_a; cm^{-3})

755 for all flights. b) N_d against N_a in the MBL for all flights, colored by maximum in-cloud

756 supersaturation (S_{max}).

757

758 **Figure 4:** The sensitivity of droplet number to a) aerosol number ($\partial N_d/\partial N_a$), b)

759 characteristic velocity ($\partial N_d/\partial w^*$), and, c) hygroscopicity parameter ($\partial N_d/\partial \kappa$) as functions

760 of N_a (cm^{-3}). The data is clustered using the "polluted", "intermediate", and "clean"

761 groupings of Table 1.

762

763 **Figure 5:** Characteristic velocity, w^*, in the MBL as a function of N_a (cm^{-3}) in the BBOA

764 plume (blue) and in the MBL (red), for each flight.

765

766   **Figure 6:** $N_d{}^{lim}$ (cm^{-3}) for each flight as a function of characteristic vertical updraft

767   velocity, $w*$ (ms$^{-1)}$. Flights are colored by "polluted", "intermediate", and "clean"

768   categories, as defined by MBL concentration. The inset also presents the "asymptotic"

769   activated droplet number ($N_d{}^{lim}$; cm^{-3}) for $w*$ ranging from 0.1 to 0.6 ms^{-1}.

770

771

772

773

774
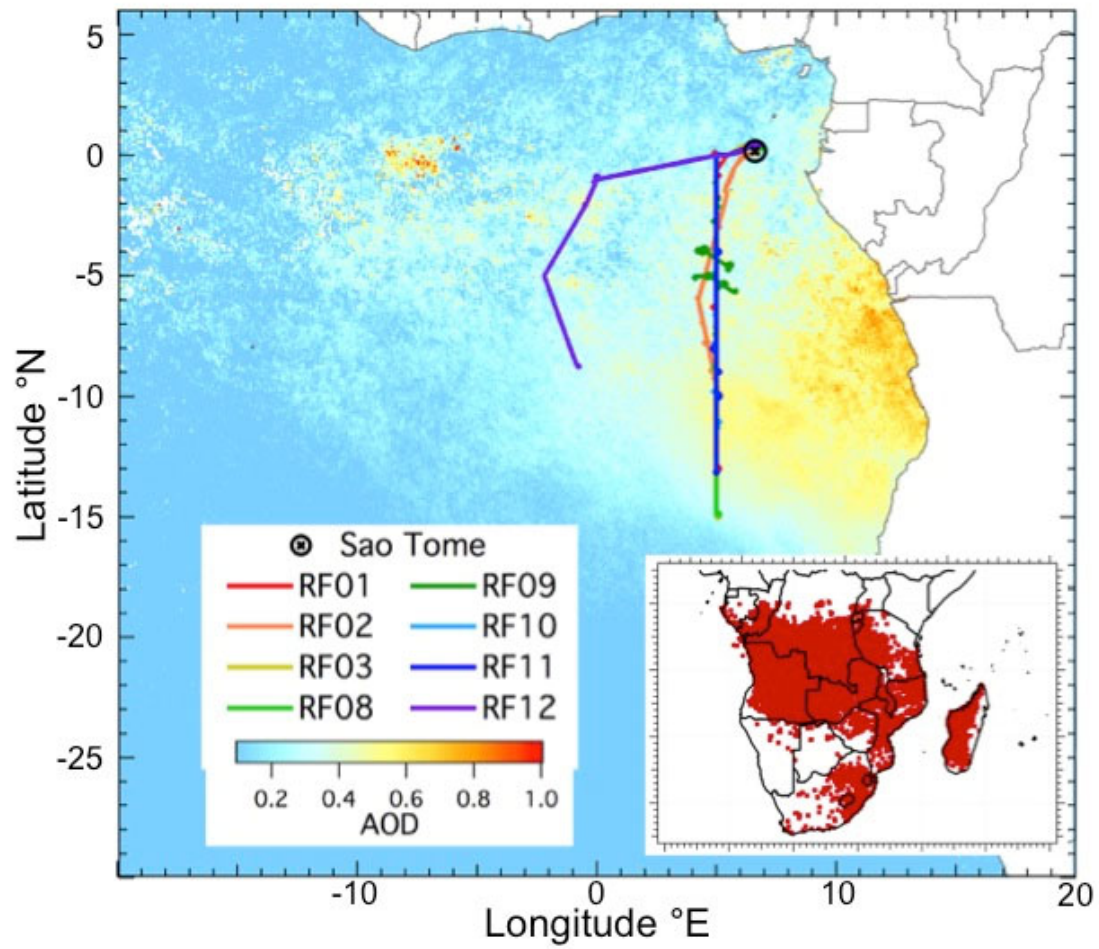
Figure 1

776

777
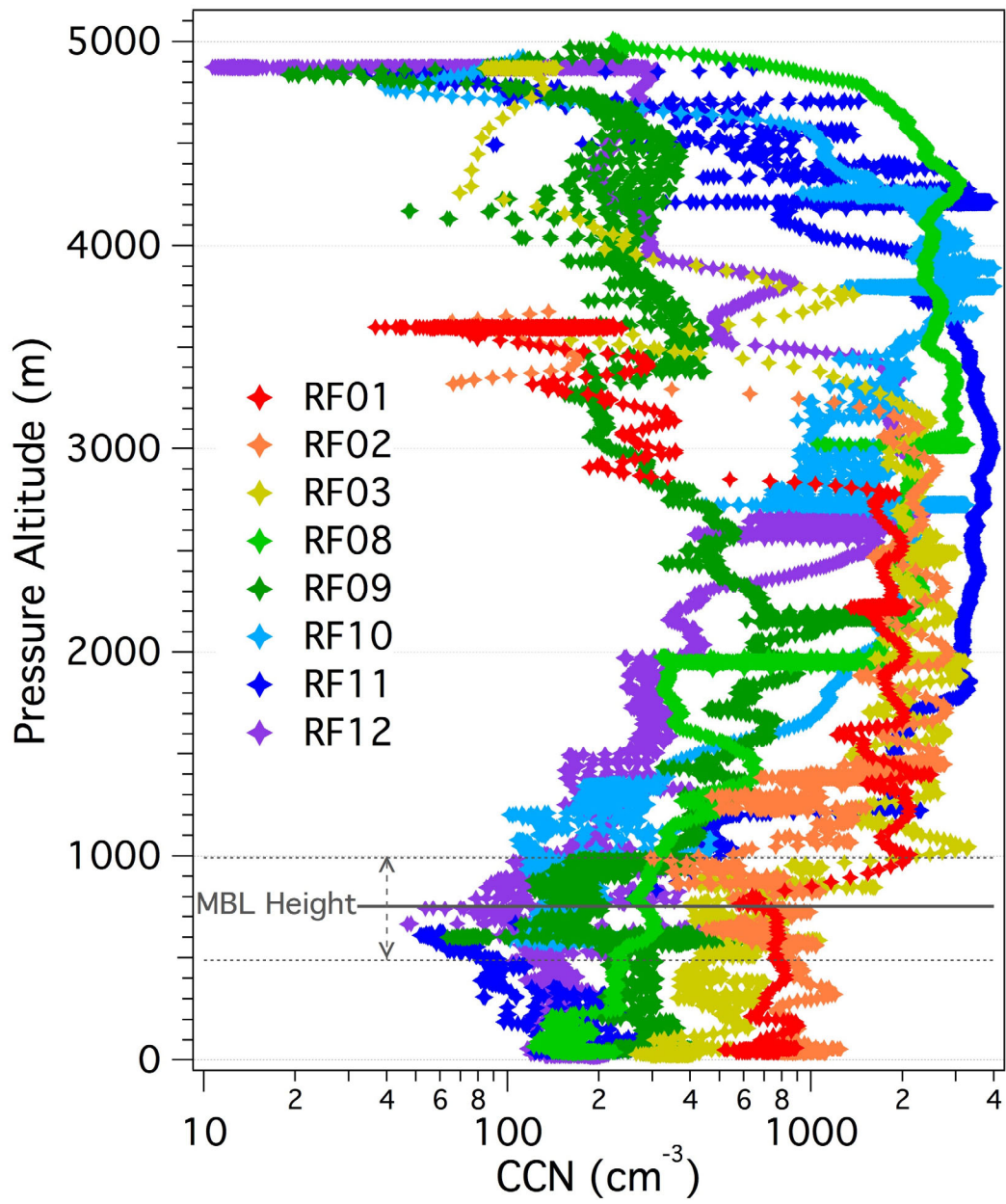
778

779

780   **Figure 2**

781

782

783
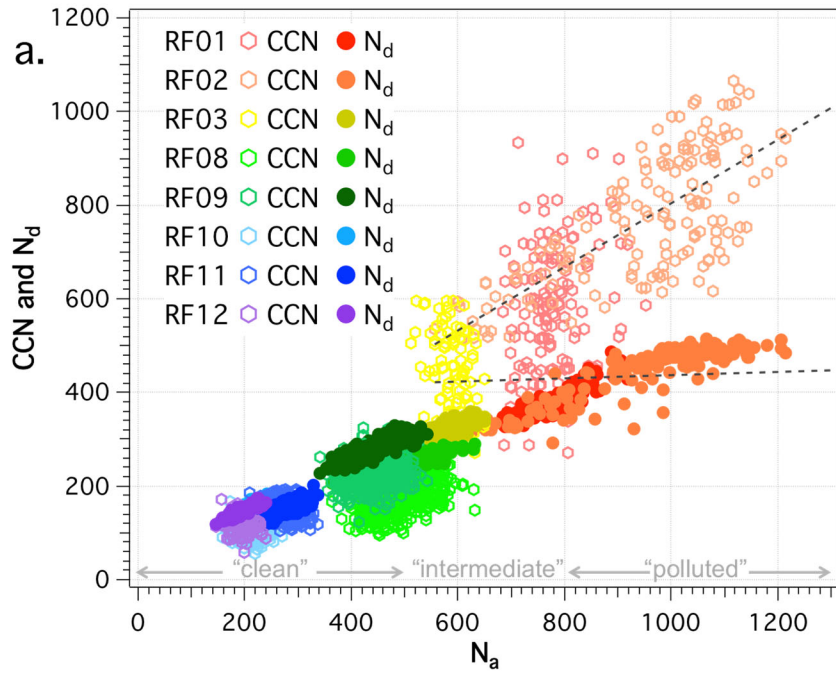
784
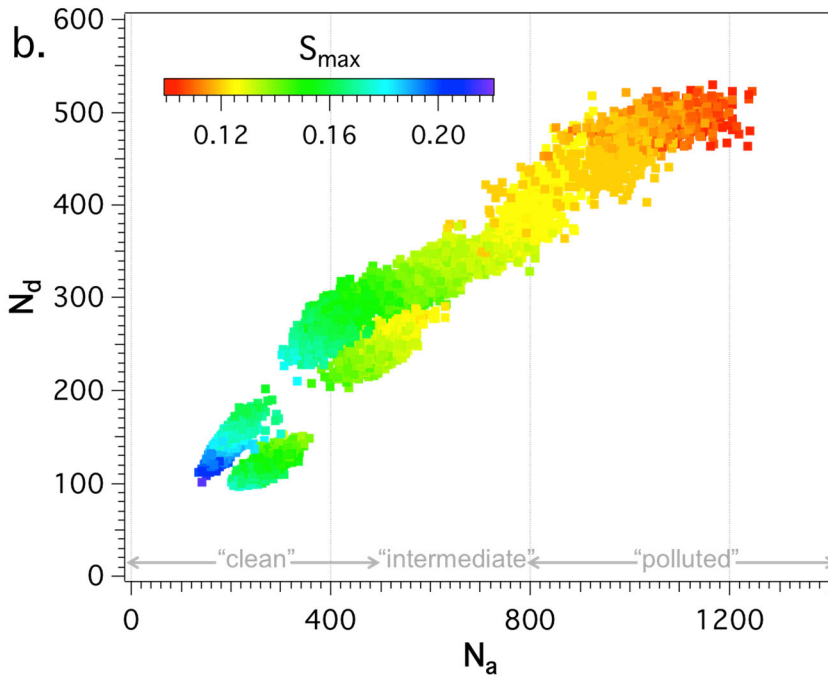
785
786
787 **Figure 3**

788

789
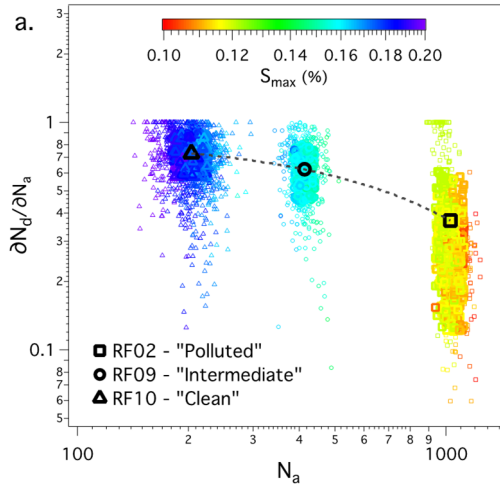
790
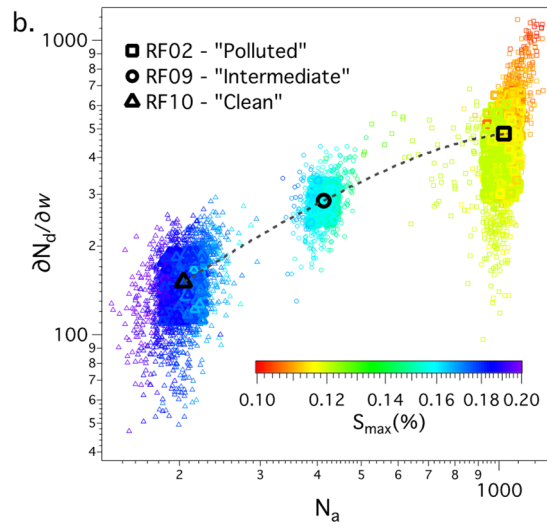
791
792   **Figure 4**

793
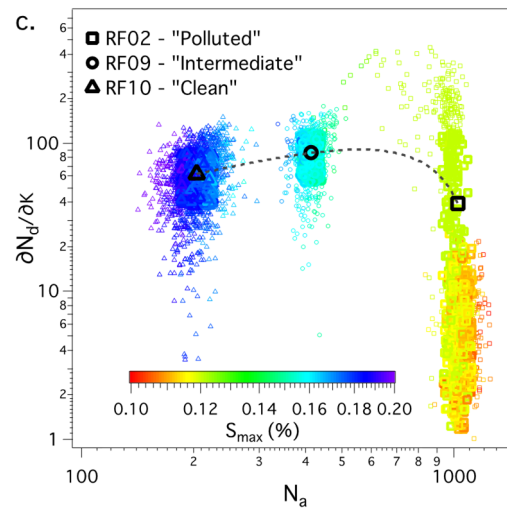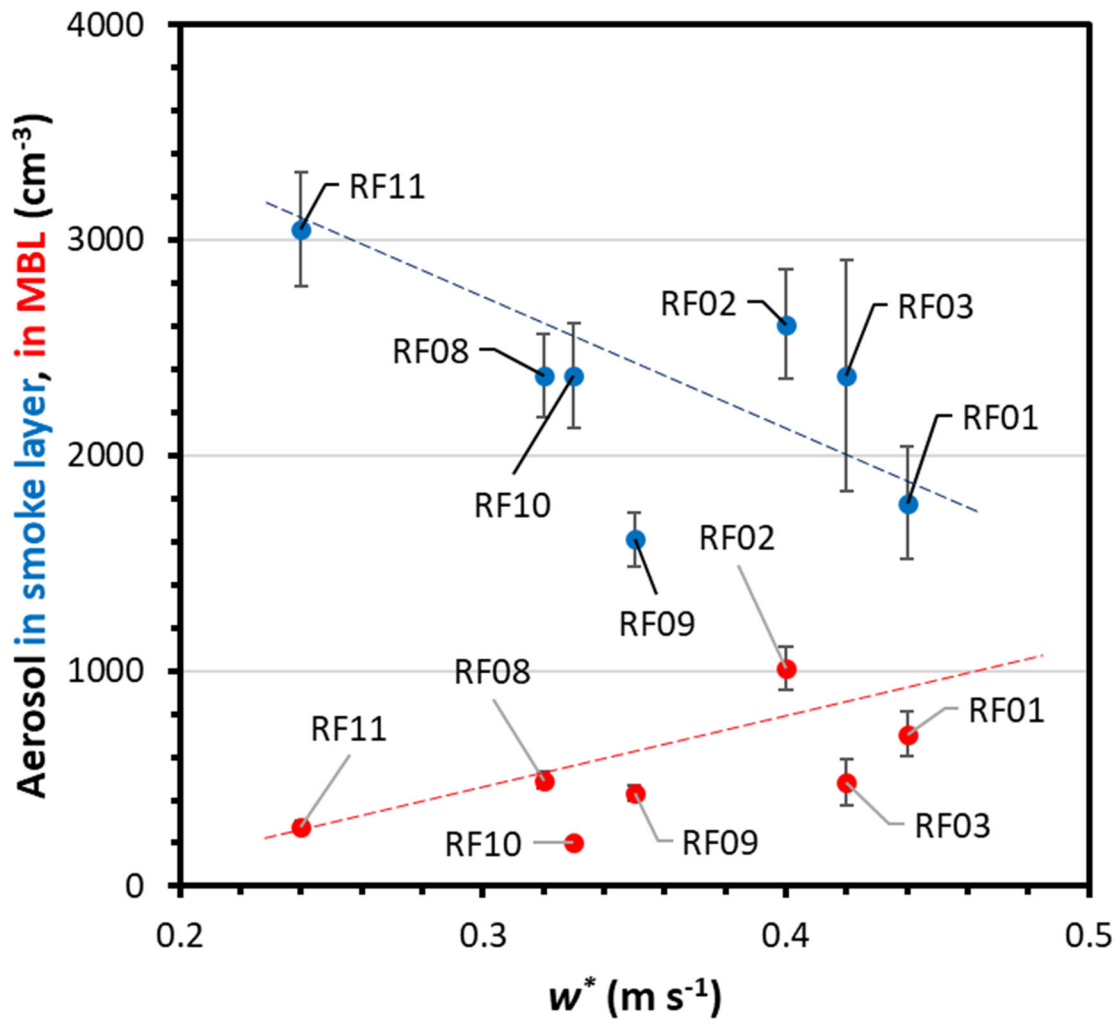
794

795

796   **Figure 5**

797

798

799

800

801   **Figure 6**

802